Characterization of Carotenoid and Chlorophyll Photooxidation in Photosystem II†

Cara A. Tracewell,‡ Agnes Cua,§ David H. Stewart,‡,|| David F. Bocian,*,§ and Gary W. Brudvig*,‡

Department of Chemistry, Yale University, P.O. Box 208107, New Haven, Connecticut 06520-8107, and Department of Chemistry, University of California, Riverside, California 92521-0403

Received August 22, 2000; Revised Manuscript Received November 2, 2000

ABSTRACT: Photosystem II (PSII) contains two accessory chlorophylls (Chl_Z, ligated to D1-His118, and Chl_D, ligated to D2-His117), carotenoid (Car), and heme (cytochrome b_{559}) cofactors that function as alternate electron donors under conditions in which the primary electron-donation pathway from the O_2-evolving complex to $P680^+$ is inhibited. The photooxidation of the redox-active accessory chlorophylls and Car has been characterized by near-infrared (near-IR) absorbance, shifted-excitation Raman difference spectroscopy (SERDS), and electron paramagnetic resonance (EPR) spectroscopy over a range of cryogenic temperatures from 6 to 120 K in both *Synechocystis* PSII core complexes and spinach PSII membranes. The following key observations were made: (1) only one Chl^+ near-IR band is observed at 814 nm in *Synechocystis* PSII core complexes, which is assigned to Chl_Z^+ based on previous spectroscopic studies of the D1-H118Q and D2-H117Q mutants [Stewart, D. H., Cua, A., Chisholm, D. A., Diner, B. A., Bocian, D. F., and Brudvig, G. W. (1998) *Biochemistry 37,* 10040−10046]; (2) two Chl^+ near-IR bands are observed at 817 and 850 nm in spinach PSII membranes which are formed with variable relative yields depending on the illumination temperature and are assigned to Chl_Z^+, and Chl_D^+, respectively; (3) the Chl and Car cation radicals have significantly different stabilities at reduced temperatures with Car^+ decaying much faster; (4) in *Synechocystis* PSII core complexes, Car^+ decays by recombination with Q_A^- and not by Chl_Z/Chl_D oxidation, with multiphasic kinetics that are attributed to an ensemble of protein conformers that are trapped as the protein is frozen; and (5) in spinach PSII membranes, Car^+ decays mainly by recombination with Q_A^-, but also partly by formation of the 850 nm Chl cation radical. The greater stability of Chl_Z^+ at low temperatures enabled us to confirm that resonance Raman bands previously assigned to Chl_Z^+ are correctly assigned. In addition, the formation and decay of these cations provide insight into the alternate electron-donation pathways to $P680^+$.

Photosystem II (PSII)[1] is a membrane-bound pigment−protein complex that is responsible for catalyzing the oxidation of H_2O to O_2 in oxygenic photosynthesis. The assembly of polypeptides that comprise PSII contains a large array of chlorophyll (Chl) molecules that collect and transfer light energy and induce photochemistry by initiating electron-transfer reactions. The PSII reaction center contains six Chls, two pheophytins (Pheos), and two β-carotenes (Cars) bound within the D1 and D2 polypeptides (*1*−*3*; reviewed in *4*) and is closely associated with a heme-containing protein, cytochrome b_{559} (Cyt b_{559}). Upon illumination, the special reaction center Chl called P680 is excited and rapidly donates an electron to a Pheo acceptor to create the charge-separated state, $P680^+$−$Pheo^-$ (reviewed in *5*). The charge separation is stabilized on the acceptor side by electron transfer from $Pheo^-$ to a bound quinone, Q_A, which is subsequently oxidized by an exchangeable quinone, Q_B. Under physiological conditions, the O_2-evolving complex, which includes a Mn_4 cluster and a redox-active tyrosine called Y_Z, is the primary electron donor to $P680^+$. However, when the primary electron-donation pathway from the O_2-evolving complex to $P680^+$ is inhibited, several alternate electron donors can be photooxidized, including an accessory Chl called Chl_Z, Car, and Cyt b_{559} (reviewed in *6*).

Because the molecular structure of PSII has not been determined at the atomic level, structural considerations of the PSII reaction center are based on analogies to the crystal structure of the non-sulfur purple bacterial photosynthetic reaction center (BRC) (*4*, *7*−*9*). These comparisons are strongly supported by recent electron crystallography of a PSII−CP47 reaction center complex at a resolution of 8 Å which indicates that the positions of both the transmembrane helices of the D1/D2 polypeptides and the chlorin cofactors of PSII are very similar to those in the BRC (*10*). The BRC

† This work was supported by Grants GM39781 (D.F.B.) and GM32715 (G.W.B.) from the National Institutes of Health, the National Research Initiative Competitive Grants Program/USDA 96-35306-3398 (G.W.B.), and National Institutes of Health Predoctoral Traineeship GM08283 (C.A.T. and D.H.S.).

* Address correspondence to either of these authors. D.F.B.: Phone, (909) 787-3660; FAX, (909) 787-4713; E-mail, dbocian@ucrac1.ucr.edu. G.W.B.: Phone, (203) 432-5202; FAX, (203) 432-6144; E-mail, gary.brudvig@yale.edu.

‡ Yale University.

§ University of California, Riverside.

|| Current address: Xanthon, Inc., 104 Alexander Dr., Research Triangle Park, NC 27709.

[1] Abbreviations: BRC, bacterial photosynthetic reaction center; Car, carotenoid; Chl, chlorophyll; CP43, 43 kDa Chl-binding protein subunit of PSII; CP47, 47 kDa Chl-binding protein subunit of PSII; Cyt b_{559}, cytochrome b_{559}; β-DM, β-dodecyl maltoside; EPR, electron paramagnetic resonance; IR, infrared; PSII, photosystem II; P680, photoactive Chl primary electron donor in PSII; Q_A, tightly bound quinone electron acceptor in PSII; RR, resonance Raman; SERDS, shifted-excitation Raman difference spectroscopy.

10.1021/bi001992o CCC: $20.00
Published on Web 12/09/2000

and the PSII reaction center are also closely related by significant protein sequence homology, 2-fold symmetry, and similar electron-transfer pathways (reviewed in *11, 12*). However, the BRC binds only four BChls and two bacteriopheophytins (BPheos), so there are two Chls in the PSII reaction center that do not have homologues in the BRC. Site-directed mutagenesis studies of PSII from *Chlamydomonas reinhardtii* (*13*−*15*) and *Synechocystis* PCC 6803 (*16*) have shown that the two additional Chls in PSII are bound in symmetric positions to D1-H118 and D2-H117, respectively.

The functional and spectroscopic characteristics of the alternate electron donors, Chl_Z and Car, have been of considerable interest recently because of the importance of these cofactors in energy regulation and utilization within PSII (*13, 14, 16*−*21*). Although spectroscopic signatures of the oxidation of the individual alternate electron donors have been identified, the locations of these components within PSII, the exact electron-transfer sequence(s) involving them, and their function are still uncertain. Early studies of primary versus alternate electron-donor oxidation indicated that Cyt b_{559} and a species giving a $g = 2.0$ radical electron paramagnetic resonance (EPR) signal were oxidized at similar rates at cryogenic temperatures relative to the Mn_4 cluster (*22*). Based on optical studies showing Chl photooxidation under these conditions (*23*), the radical was assigned as Chl_Z^+ (*24*). Combined with the preferential photooxidation of Cyt b_{559} over Chl at low temperatures (*24*), this observation led to the proposal of a linear path of electron transfer from Cyt b_{559} to Chl_Z to $P680^+$ (*22*). Because Cyt b_{559} can be reduced by Q_B^- (*25*), these species could allow for cyclic electron transfer within PSII. A number of functional roles have been attributed to the alternate electron donors, most involving participation in mechanisms of protection against photoinhibition (*6*). For example, oxidized Chl_Z has been identified as a potent quencher of fluorescence (*19*) that may act in concert with Cyt b_{559} to dissipate excess energy under conditions of high light stress (*26*).

Studies of site-directed mutants have been carried out in order to determine the amino acid residue coordinated to the redox-active Chl_Z. Initial EPR studies of the distance between Chl_Z^+ and the non-heme Fe(II) associated with the electron acceptors Q_A and Q_B pointed to the D1-H118 and D2-H117 residues (*18*). Resonance Raman (RR) spectroscopic studies of *Synechocystis* PSII core complexes isolated from the D1-H118Q and D2-H117Q mutants demonstrated that D1-H118 is the ligand of the redox-active Chl (Chl_Z) and D2-H117 is the ligand of the redox-inactive Chl (Chl_D) (*16*). On the other hand, site-directed mutagenesis studies of these two residues carried out in *Chlamydomonas reinhardtii* have implicated D2-H117 as the ligand to a redox-active accessory Chl (*14*). It is unresolved whether the different conclusions stem from a problem with the spectroscopic assignments or from a species-dependent difference in the redox properties of the two accessory Chls.

It has also been observed that Car can be photooxidized at low temperatures. In the original report (*27*), the yield of Car^+ was very low unless a lipophilic anion, such as ANT2p, was added. Because such lipophilic anions can act as redox mediators (*28*), the prevailing view was that Car photooxidation was not intrinsic to untreated PSII. More recently, however, it has been demonstrated that Car can be photooxidized in high yield in PSII preparations that undergo normal electron-transfer reactions (*29*−*31*). This has led to several new proposals for alternate electron transfer including linear and branched pathways (*30*−*32*). All of the proposals assign Car as the direct reductant of $P680^+$ and as an electron-transfer intermediate between $P680^+$ and Cyt b_{559} and/or Chl_Z, an assignment that is consistent with the relatively large distances between Chl_Z/Cyt b_{559} and P680. Chl_Z is about 30 Å away from P680 (*10, 16, 17*), and the Cyt b_{559} heme is positioned on the stromal side of the membrane, opposite that of P680 (*10, 33, 34*). Because electron-transfer rates are strongly dependent on distance, electron transfer from Cyt b_{559} or Chl_Z to $P680^+$ is expected to be inefficient without an intermediate redox-active species.

In this work, the temperature dependence of the formation and decay of Chl_Z^+ and Car^+ is characterized in both spinach PSII membranes and *Synechocystis* core complexes by near-infrared (near-IR) absorbance, EPR spectroscopy, and shifted-excitation Raman difference spectroscopy (SERDS). For both types of samples, low-temperature illumination generates a mixture of Chl and Car cation radicals. The Car^+ species is less stable toward recombination, consistent with the redox-active Car being the direct reductant to $P680^+$ and closer to the core of the reaction center. The properties of the Chl cation radicals are, however, significantly different in the two species. In spinach PSII, two different Chl cation radicals are observed having near-IR peaks at 817 and 850 nm, respectively, whereas in *Synechocystis* PSII, only one Chl cation radical with a peak at 814 nm is observed. In addition, no interconversion between Car^+ and Chl_Z^+ occurs upon warming a preilluminated sample in the dark from 6 to 120 K in *Synechocystis* PSII, whereas such a warming yields some formation of the 850 nm Chl cation radical from Car^+ in spinach PSII. The temperature dependence for formation and interconversion of these radical species provides insight into the functional mechanism of alternate electron donation in PSII and contrasts with previous work using other PSII preparations. In addition, these studies allow for the definitive assignment of resonance Raman bands associated with Chl_Z^+.

MATERIALS AND METHODS

PSII core complexes were isolated from *Synechocystis* PCC 6803, and PSII-enriched membranes were prepared from market spinach as described previously (references *16* and *35*, respectively). Oxygen-evolving rates were measured using a Clark-type electrode and were typically between 1400 and 2300 μmol of O_2 (mg of Chl)$^{-1}$ h^{-1} for *Synechocystis* and 400−450 μmol of O_2 (mg of Chl)$^{-1}$ h^{-1} for spinach samples. Manganese depletion of the PSII preparations was performed by a 30 min incubation while stirring on ice in buffer A [50 mM 2-(*N*-morpholino)ethanesulfonic acid (MES), 15 mM NaCl, 1 mM $CaCl_2$, 5 mM sodium ethylenediaminetetraacetate (Na_4EDTA), 0.4 M sucrose, and 0.03% β-dodecyl maltoside (β-DM) at pH 6.5] containing 10 mM hydroxylamine. Hydroxylamine and free manganese ions were removed by two cycles of concentration and resuspension in buffer A using an Ultrafree-4 concentrator (Millipore, 100 kDa nominal molecular mass cutoff). Finally, the core complexes were resuspended in a buffer containing 60% glycerol, 50 mM MES, and 0.03% β-DM, and a 100-fold excess of potassium ferricyanide relative to the PSII concentration was added to oxidize Cyt b_{559}. Spinach PSII

membranes were resuspended in the same buffer excluding β-DM. The added ferricyanide also oxidizes Q_A^-; direct optical and EPR measurements show that there is no Q_A^- in the dark-adapted samples (*36*). Chl concentrations were measured by methanol extraction using the extinction coefficient of 79.24 mL (mg of Chl)$^{-1}$ cm^{-1} at 665 nm. PSII concentrations used in the near-IR absorption experiments were 5.7 and 8.7 mg of Chl/mL for *Synechocystis* and spinach samples, respectively. These concentrations correspond to 170 μM PSII for *Synechocystis* core complexes based on 38 Chls/PSII (*37*) and 48 μM PSII for spinach PSII membranes based on 200 Chls/PSII (*25*).

Near-IR Optical Spectroscopy. Low-temperature optical spectra were measured on samples in a home-built Plexiglas flat cell with a path length of 1.25 mm. Two cryostats were used for low-temperature experiments: a home-built nitrogen-flow cryostat over the temperature range 85−120 K or an Oxford ESR 900 He-flow cryostat for measurements at lower temperatures. Uncracked glasses of the PSII samples were made by cooling the sample slowly above liquid nitrogen followed by transfer to the helium cryostat or by cooling the sample inside the nitrogen cryostat with a typical rate of 0.1 °C/s. The sample was kept in the dark as it was cooled and also for 30 min at the illumination temperature to equilibrate. Steady-state accumulations of the cation radical species were generated by 15 min illumination of the sample inside the specified cryostat using white light from a 200 W quartz halogen lamp filtered with a 6 in. water bath and a heat-absorbing filter (Schott KG-5) and directed to the sample through a fiber optic unless otherwise noted. Previous work has shown that illumination below 150 K for up to 2 h does not photodamage the samples (*19*). Near-IR spectra of the photogenerated cation radicals were collected immediately following illumination on a Perkin-Elmer Lambda-20 UV−vis spectrophotometer. For warming experiments, the samples were brought to the desired incubation temperature inside the cryostat over a period of about 2 min, and then the time of incubation in the dark was started. At the end of the incubation, the sample was brought back to the measurement temperature over a period of about 2 min, and the spectrum was recorded. Spectra were scanned from long to short wavelengths at a rate of 240 nm/min unless otherwise specified.

The overlapping near-IR absorption spectra from the Car and Chl cation radicals were analyzed by Gaussian deconvolution using Microcal Origins 6.0. Data points for the time course of decay of the cation radicals during dark incubations were obtained by using the maxima of Gaussians obtained by deconvolution of background-corrected near-IR absorption spectra.

EPR Spectroscopy. X-band EPR measurements were conducted on a Varian E-9 spectrometer equipped with an Oxford ESR 900 He-flow cryostat and a TE_{102} cavity operating at a frequency of 9.29 GHz. Each spectrum is an average of 4 scans collected under the following nonsaturating conditions. The overlapping Car^+/Chl^+ radical signals at $g \sim 2.00$ were measured at 30 K, using 0.02 mW power, 4.0 G modulation amplitude, and 100 kHz modulation frequency. Then the sample was cooled to 5 K, and the $Fe^{2+}-Q_A^-$ signal at $g \sim 1.9$ was measured using 5.0 mW power, 20.0 G modulation amplitude, and 100 kHz modulation frequency. PSII samples were dark-adapted prior to illumination. Cation radicals were generated by 15 min illumination at 30 K with a 200 W quartz halogen lamp. All spectra were collected in the dark. For the measurements of radical decay in the dark, the sample was incubated in the cryostat at 30 K during the intervals between scans. Radical yields were determined by double integration of the derivative EPR signals and calibrated to the quantity of oxidized tyrosine D ($Y_D^\bullet$) generated in the sample from 1 min illumination at 0 °C, followed by freezing in the dark to 77 K. The intensity of the $Fe^{2+}-Q_A^-$ signal was measured from the maximum-to-minimum amplitude of the derivative signal.

RR Spectroscopy. The RR measurements were made at 30 K on highly concentrated (∼10 mg/mL) glassy samples (40% v/v glycerol) contained in 1 mm i.d. capillary tubes. The sampling accessories, spectrometer, and laser systems have been previously described (*38, 39*). Each RR data set was obtained with 40 min (20 × 120 s) of signal averaging. Cosmic spikes in the individual scans were removed prior to coaddition of the scans. The excitation wavelength was 820 nm; the laser power was ∼5 mW; the spectral resolution was ∼2 cm^{-1}. All spectra are unpolarized. The spectral data were calibrated using the known frequencies of fenchone. Both nonilluminated and illuminated spectra were collected for the PSII samples. Illumination consisted of exposure to continuous white light from a focused 200 W quartz/halogen lamp for 15 min.

The RR spectra were acquired using the shifted-excitation Raman difference spectroscopic (SERDS) technique in order to reduce the level of interference from fluorescence (*40, 41*). The application of the SERDS method to PSII (*16, 42*) and other photosynthetic proteins has been previously described in detail (*40, 43*−*49*). Briefly, each data set is acquired at two excitation wavelengths which differ by a small wavenumber increment (∼10 cm^{-1}). The 40 min data acquisition times indicated above are for each of the two data sets required to construct the SERDS traces. These data sets are subtracted to yield a background-free RR difference (SERDS) spectrum. The RR spectra presented herein were obtained by subtracting the initial spectrum from the shifted spectrum. The spectral window is defined by the initial spectrum and corresponds to the wavenumber axis in the figures.

RESULTS

Near-IR optical spectra of *Synechocystis* Mn-depleted PSII core complexes and spinach Mn-depleted PSII membranes following illumination at temperatures from 6 to 120 K are shown in Figure 1. Spectra taken after warming the 30 K-illuminated samples in darkness to 77 or 120 K are shown in Figure 2. The preillumination scans showed no radical cations present in the sample. A Gaussian deconvolution was performed to determine the number of components contributing to the spectra and their intensities. It was found that three Gaussians with peak maxima of 814, 878, and 987 nm were sufficient to reproduce the spectra from *Synechocystis* Mn-depleted PSII core complexes (Figure 1C), whereas four Gaussians with peak maxima of 817, 850, 895, and 994 nm were required to reproduce the spectra from spinach Mn-depleted PSII membranes (Figure 1D).

The peaks at 987 nm (*Synechocystis*) and 994 nm (spinach) are from Car^+ and agree with results reported previously (*27*,

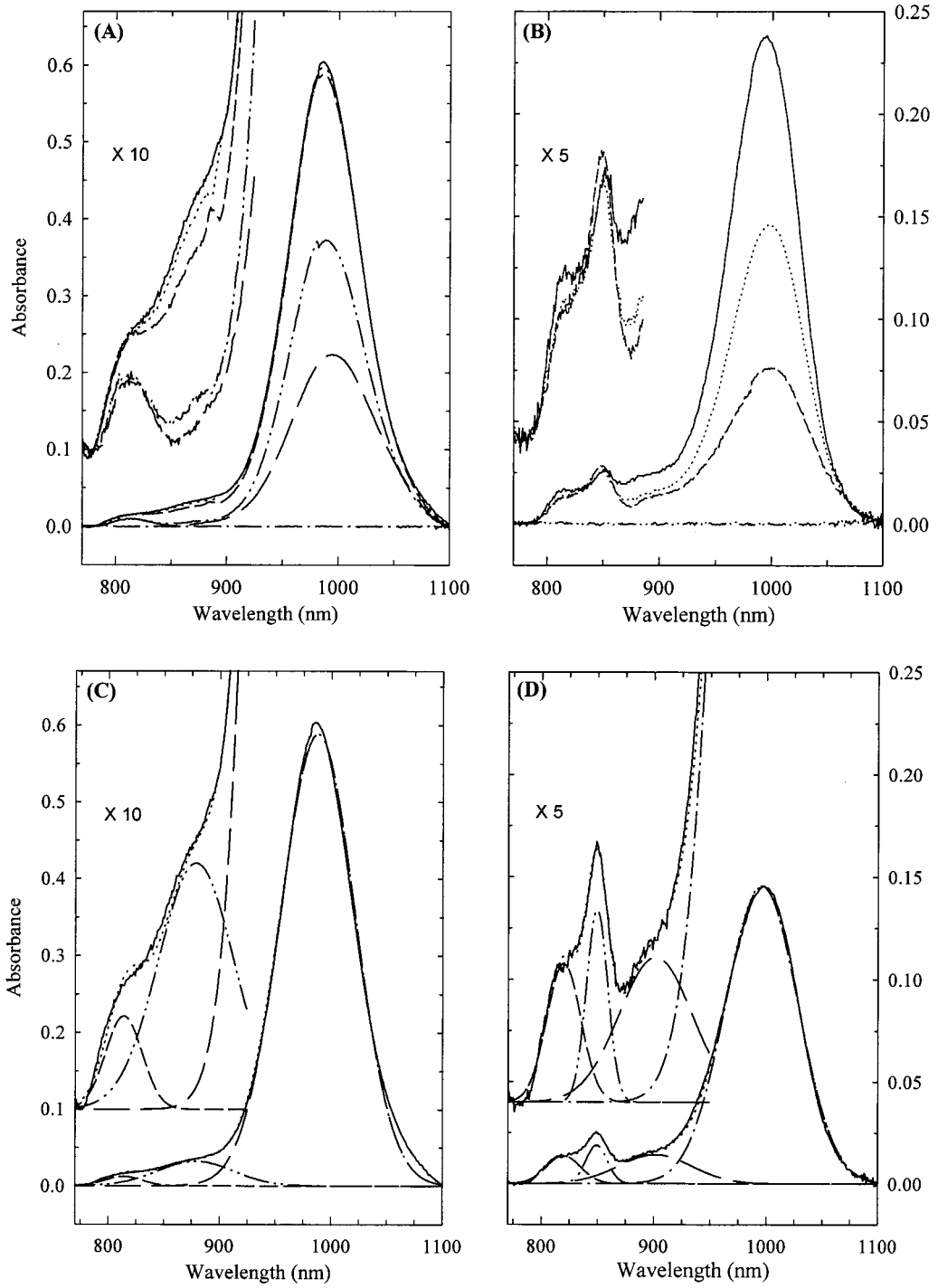

FIGURE 1: Near-IR absorption spectra for Mn-depleted *Synechocystis* (A and C) and spinach PSII (B and D). Shown in (A) are spectra from *Synechocystis* PSII collected after 15 min illumination at 6 K (solid), 20 K (dotted), 30 K (dashed), 85 K (dash−dot−dot), and 120 K (long dash). Shown in (B) are spectra from spinach PSII collected after 15 min illumination at 30 K (solid), 85 K (dotted), and 120 K (dashed). Illuminations were performed at the same temperature at which the spectra were collected. Preillumination spectra (bottom trace in panels A and B) show no cations are present. Panels C and D show Gaussian deconvolutions of absorption spectra collected after 15 min illumination at 6 K (*Synechocystis*) and 85 K (spinach), respectively. Spectra for *Synechocystis* PSII are fit by three Gaussian line shapes; traces shown are the absorption spectra (solid), fit (dotted), Chl_Z^+ band (dashed), Car^+ vibronic band (dash−dot−dot), and Car^+ band (long dash). Spectra for spinach PSII are best described by four Gaussian line shapes (see text for details); traces shown are the absorption spectra (solid), fit (dotted), two Chl^+ electronic bands at 817 nm (dashed) and 850 nm (dash−dot−dot), vibronic band of Car^+ (long dash) and Car^+ band (dash−dot). Magnification of the Chl^+ region is shown in all panels.

30). As discussed in (*30*), the wavelength maximum is characteristic of a β-carotene cation radical in which the hole is delocalized over all 11 of the double bonds. The peaks at 878 nm (*Synechocystis*) and 895 nm (spinach) were found to mirror the intensity of the main Car^+ bands and exhibited the same decay kinetics during the dark-incubation experiments shown in Figure 3 (data not shown), suggesting that these weaker features are Car^+ vibronic bands. This assignment also fits with the shift of ~1100−1200 cm^{-1} of these satellite bands from the main Car^+ band which matches the frequency of the strong ν_2 modes observed in the RR spectrum of Car^+ (*30*). It is interesting that there is a small

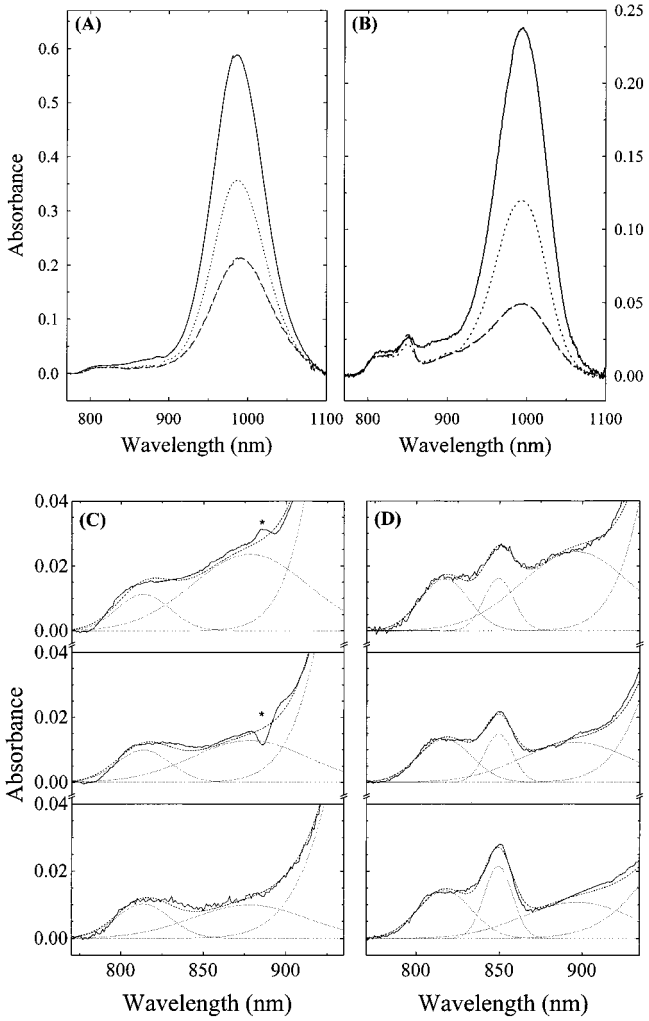

FIGURE 2: Warming experiment for Mn-depleted *Synechocystis* (A and C) and spinach PSII (B and D). Shown in (A) and (B) are spectra collected after 15 min illumination at 30 K (solid), followed by 30 min incubation in the dark at 77 K (dotted) or 120 K (dashed). All spectra were collected at 30 K. Panels C and D show Gaussian deconvolutions of spectra shown in (A) and (B), respectively. For clarity, each spectrum and the corresponding fit are presented in separate panels: 30 K illumination (upper panel), incubation at 77 K (middle panel), and incubation at 120 K (lower panel). Fitting the spectra (solid) with three (*Synechocystis* PSII) or four (spinach PSII) Gaussian curves (dotted) which have a fixed peak position and width produced the simulated spectra (dashed). Peak maxima are 814, 878, and 987 nm for *Synechocystis* PSII spectra, and 817, 850, 895, and 994 nm for spinach PSII spectra. The asterisk indicates an anomalous feature in the spectra around ~890 nm produced by a grating change as the spectrometer scans through this region.

blue-shift of both the Car^+ fundamental and vibronic bands in *Synechocystis* compared to those in spinach PSII, which provides further evidence in support of the assignment of the bands at 878 and 895 nm as Car^+ vibronic bands, and indicates that the protein environments are slightly different in the two organisms.

The peaks at 814 nm (*Synechocystis*) and 817/850 nm (spinach) are characteristic of Chl cation radicals and also agree with results reported previously (*16*, *31*). There is obviously a significant difference between the two species in that an extra Chl cation radical peak is present in the spinach sample. It has been observed in model systems that Chl cation radicals can exhibit a double maximum in the

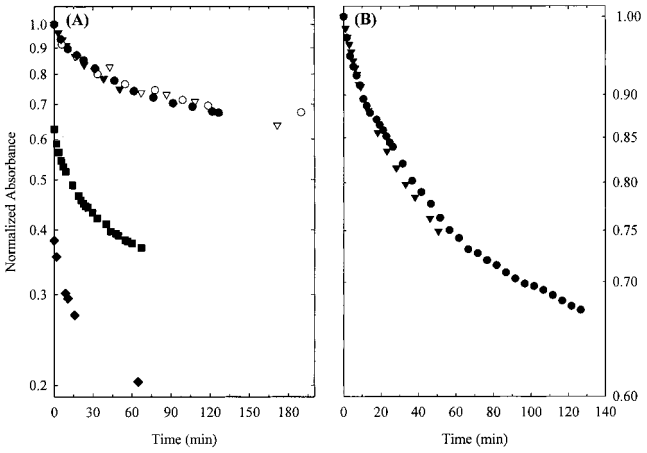

FIGURE 3: (A) Near-IR absorbance and EPR measurement of the dark decay of the cation radicals formed by illumination of Mn-depleted *Synechocystis* PSII. Car^+ near-IR data obtained at 6 K (filled circles), 30 K (filled triangles), 85 K (filled squares), and 120 K (filled diamonds). The illuminations were performed at the same temperature at which the spectra were collected. Data are normalized to the initial absorption measured for the 6 K experiment (0.603). Because of overlap, only every third data point is plotted for the Car^+ near-IR data obtained at 6 and 30 K. EPR data for decay in the dark at 30 K of the superimposed Car^+ and Chl_Z^+ signals (open circles) and $Fe^{2+}-Q_A^-$ signal (open triangles). For description of EPR experiment, see text. (B) Car^+ near-IR data from panel A obtained at 6 K (filled circles) and 30 K (filled triangles) plotted on an expanded absorbance scale and including all of the data points.

near-IR (*50*). However, this appears not to be the correct interpretation for the double maximum from the Chl cation radicals in spinach PSII because the 817 and 850 nm peaks are formed with different yields depending on the experimental conditions (Figure 2D). Instead, it appears that two different Chl cation radicals are formed in spinach PSII, whereas only a single Chl cation radical is formed in *Synechocystis* PSII.

We have used extinction coefficients from previous studies of model complexes, together with Gaussian deconvolutions of the absorption bands, to estimate the yield of each radical cation. The results are shown in Table 1. These yields are approximate values because the extinction coefficients for the PSII radicals are not known precisely. For Car^+, an extinction coefficient of 160 000 M^{-1} cm^{-1} was used (*51*). However, the different line shapes for the 814/817 and 850 nm Chl cation radicals make the Chl^+ extinction coefficients less certain. We used an extinction coefficient of 7000 M^{-1} cm^{-1} for the 814/817 nm Chl cation radical (*52*). For the 850 nm Chl cation radical, the extinction coefficient was estimated based on an extinction coefficient of 7000 M^{-1} cm^{-1} for the 814/817 nm Chl cation radical and the assumption that the Gaussians fit to the two Chl^+ near-IR bands have equal areas for equal concentrations of the radicals. This yielded an extinction coefficient of 12 600 M^{-1} cm^{-1} for the 850 nm Chl cation radical, which agrees with previously reported values for Chl *a* cation radicals (*53*, *54*). A measure of the reliability of the yield estimates can be obtained by comparison to previous EPR quantitations of the radical yields under the same conditions. It is expected that the maximum total radical yield should be close to 1.0 per center because the other electron donors (Cyt b_{559} and the Mn_4 cluster) are not active in preoxidized Mn-depleted samples and PSII is restricted by the electron-acceptor side

Table 1: Cation Radical Yields following 15 min Illuminations and Subsequent Dark-Incubations

	illumination conditions		radical yield per PSII			
PSII sample	illumination temp	incubation in dark	Car^{+} [a]	Chl^{+} [b] (814/817 nm)	Chl^{+} [c] (850 nm)	total
Synechocystis	6 K	–	0.37	0.15	0	0.52
	20 K	–	0.37	0.15	0	0.52
	30 K	–	0.36	0.14	0	0.50
	30 K	30 min at 77 K	0.22	0.12	0	0.34
	30 K	30 min at 120 K	0.13	0.12	0	0.25
	85 K	–	0.23	0.10	0	0.33
	120 K	–	0.14	0.11	0	0.25
spinach	30 K	–	0.46	0.43	0.24	1.13
	30 K	30 min at 77 K	0.24	0.37	0.22	0.83
	30 K	30 min at 120 K	0.10	0.38	0.32	0.80
	85 K	–	0.28	0.32	0.27	0.87
	120 K	–	0.15	0.31	0.35	0.81

[a] Based on an extinction coefficient of 160 000 M^{-1} cm^{-1} for the carotenoid cation radical (*51*). [b] Based on an extinction coefficient of 7000 M^{-1} cm^{-1} for the 814/817 nm chlorophyll cation radical (*52*). [c] Based on an extinction coefficient of 12 600 M^{-1} cm^{-1} for the 850 nm chlorophyll cation radical (see Results).

to one stable charge separation at low temperature. In agreement with this expectation, EPR studies have shown that the radical yield per preoxidized Mn-depleted PSII following illumination at 77 K is 0.95 in spinach PSII membranes (*24*) and 0.81 in *Synechocystis* PSII core complexes (*55*). The yields estimated optically are shown in Table 1. The total radical yield estimated optically is lower in *Synechocystis* compared to spinach PSII, as was also observed in the EPR measurements. However, the total radical yields estimated optically (for samples illuminated at 85 K) are lower than the yields obtained by EPR measurements (for samples illuminated at 77 K) in both *Synechocystis* and spinach PSII. This is most likely due to a greater extent of radical decay prior to the optical measurements. Generally, for both *Synechocystis* and spinach Mn-depleted PSII, the yield of each cation radical is lower at the warmer illumination temperatures and after dark-incubation owing to charge-recombination reactions (see below). Differences between the optical and EPR quantitations may also be due to uncertainty in the optical extinction coefficients

The time course for formation of the cation radicals during illumination at 30 K was also studied. Illumination times of 1 min or less gave incomplete formation of the radical cations, but still yielded a mixture of Chl and Car radicals (data not shown). To study whether there is a thermal barrier for formation of Chl^{+} from Car^{+}, near-IR spectra were measured before and after warming the samples in the dark. Figure 2 shows near-IR optical spectra obtained by illumination at 30 K followed by warming to 77 and 120 K in the dark and recooling to 30 K, where the optical spectra were recorded. The data clearly show decay of Car^{+} in both *Synechocystis* and spinach PSII samples upon warming in the dark, as observed previously in spinach PSII (*31*). However, the decay of Car^{+} did not occur with concomitant formation of Chl_Z^{+}, as observed previously in spinach PSII (*31*), although the results were somewhat different between the *Synechocystis* and spinach PSII samples.

In the *Synechocystis* PSII samples, warming caused both Car^{+} and Chl_Z^{+} to decay. However, the extent of decay of Car^{+} was much greater. Warming the sample in the dark to 120 K for 30 min resulted in decay of 64% of Car^{+} but only 14% of Chl_Z^{+} (Figure 2C and Table 1). As shown below, the decays occur by charge recombination. Therefore, these results indicate that $Car^{+}Q_A^{-}$ is a less stable charge separation than $Chl_Z^{+}Q_A^{-}$.

For spinach PSII membranes, two Chl^{+} peaks are observed in the near-IR, and the two exhibited different behavior in the warming experiments. The 817 nm Chl cation radical exhibited very similar changes to those of Chl_Z^{+} in *Synechocystis* PSII; warming caused a small extent of decay of the 817 nm Chl cation radical peak (Figure 2D). However, the yield of the 850 nm Chl cation radical increased by about 30% when a spinach PSII membrane sample was warmed in the dark to 120 K for 30 min. As shown in Table 1, the amount of Car^{+} that decayed upon warming was significantly larger (78%) than the amount of the 850 nm Chl cation radical formed, indicating that Car^{+} decays mainly by recombination with Q_A^{-}, but also partly by formation of the 850 nm Chl cation radical in the spinach samples.

To determine the mechanism for the decay of the Car and Chl cation radicals, the decay reactions were studied by both near-IR optical and EPR spectroscopies over a range of temperatures. Figure 3 shows the time course for dark decay of the cation radical species generated by low-temperature illumination of *Synechocystis* Mn-depleted PSII samples. Decay of Car^{+} was measured by near-IR absorbance spectroscopy at 6, 30, 85, and 120 K. These optical data are normalized to the initial Car cation radical absorbance generated by the 30 K steady-state illumination. Data points of the decay traces were obtained by fitting a Gaussian curve to the baseline-corrected Car^{+} near-IR absorbance; the Gaussian maxima are plotted on a log scale in Figure 3. Figure 3B shows the 6 and 30 K Car^{+} decay traces on an expanded absorbance scale. This decay trace can be described by primarily two exponential decay components. Examination of the Car^{+} decay data at warmer temperatures reveals additional fast exponential decay components. Multiple exponential decay components show that the samples are inhomogeneous with respect to the microscopic decay rate constants.

Because the decay of Car^{+} in *Synechocystis* PSII did not occur with concomitant formation of Chl_Z^{+}, it was expected that recombination of the $Car^{+}Q_A^{-}$ charge-separated state is the likely mechanism for decay of Car^{+}. To examine this possibility, EPR spectroscopy was used to measure the time

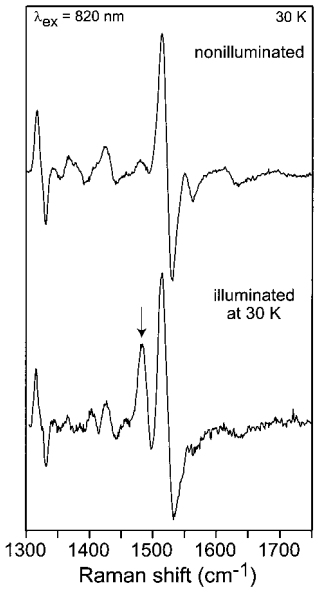

FIGURE 4: High-frequency near-IR-excitation SERDS data for nonilluminated (top trace) and illuminated (bottom trace) Mn-depleted *Synechocystis* PSII core complex obtained at 30 K. The illumination was performed at 30 K. The feature at ~1480 cm^{-1} (marked by the arrow) in the spectrum of the illuminated sample is a benchmark for the formation of Chl_Z^+.

course for decay of the radical species and Q_A^-. The X-band EPR signals from Car^+ and Chl^+ are unresolved. However, the integrated EPR signal intensity can be used to determine whether the decay of Car^+ occurs via oxidation of Chl or via charge recombination. In the former case, the integrated radical EPR signal intensity would not change, whereas in the latter case, it would decrease. As shown in Figure 3, the radical EPR signal intensity decays, and the time course is the same as the decay of the 987 nm absorbance from Car^+. Similarly, the $Fe^{2+}-Q_A^-$ EPR signal decays concurrently with the combined Car^+/Chl_Z^+ EPR signal and the near-IR absorption from Car^+. Collectively, these results show that dark incubation of *Synechocystis* PSII following illumination at 30 K leads to recombination of the $Car^+Q_A^-$ charge-separated state rather than hole transfer from Car^+ to Chl_Z.

To confirm the effect of warming the sample in the dark on the redox state of Chl_Z^+, we have used near-IR-excitation resonance Raman spectroscopy, a technique that was previously shown to measure this cation radical selectively (*42*). The near-IR-excitation SERDS data obtained for Mn-depleted *Synechocystis* PSII core complexes are shown in Figures 4−6. [Reliable SERDS data could not be obtained for spinach PSII because the fluorescence level is much higher owing to the larger number of Chls in the complex.] Figure 4 shows the high-frequency SERDS traces obtained for nonilluminated and illuminated samples at 30 K. These data are identical to those we have previously reported for Mn-depleted PSII (*16*, *42*). The fits of the SERDS data and the RR spectra reconstructed from these data have been reported elsewhere and will not be reproduced here (*16*, *42*). The salient observation depicted in Figure 4 is that illumination of Mn-depleted PSII at 30 K generates a number of new RR features. The most prominent of these features is the strong band at ~1480 cm^{-1} (marked by the arrow). We have previously assigned the illumination-induced RR bands to Chl_Z^+ (*16*, *42*). The RR bands that are common to both the nonilluminated and illuminated spectra are attributed to

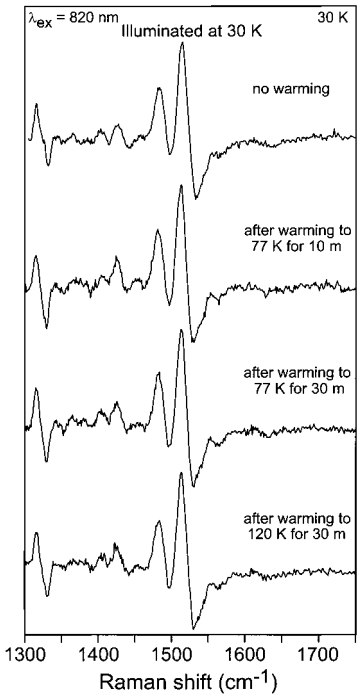

FIGURE 5: High-frequency near-IR-excitation SERDS data for illuminated Mn-depleted *Synechocystis* PSII core complex obtained at 30 K after warming to various temperatures: no warming (top trace), after warming to 77 K for 10 min (second trace), after warming to 77 K for 30 min (third trace), after warming to 120 K for 30 min (bottom trace). The illumination was performed at 30 K.

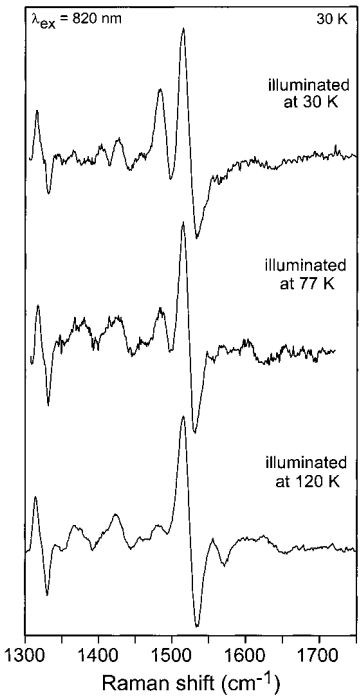

FIGURE 6: High-frequency near-IR-excitation SERDS data for Mn-depleted *Synechocystis* PSII core complex obtained at 30 K after illumination at 30 K (top trace), 77 K (middle trace), and 120 K (bottom trace).

preresonance Raman scattering from the large number of neutral Chl cofactors in the PSII core complex.

Figure 5 shows the SERDS data obtained for Mn-depleted PSII after illumination at 30 K, warming to either 77 or 120

K in the dark, and then returning to 30 K where the RR data were acquired. The top trace is the control and shows the SERDS data obtained for a sample that has been dark-adapted for ~10 min, but has not been warmed from the illumination temperature of 30 K. These data are identical to those shown for the illuminated sample in Figure 4 (bottom trace). The second and third traces in Figure 5 are SERDS data obtained after warming the sample to 77 K for 10 and 30 min, respectively. The bottom trace shows the SERDS data obtained after warming to 120 K for 30 min. Inspection of the data obtained for the warmed samples reveals that equilibration at the elevated temperatures does not result in any significant loss of the RR signals formed by illumination (e.g., those attributed to Chl_Z^+). In addition, no new spectral features are observed in the samples that have been equilibrated at elevated temperatures. Indeed, the SERDS data obtained for the warmed samples are essentially identical to those obtained for the illuminated sample that has been maintained at 30 K (Figure 5, top trace). These results are consistent with the interpretation that the illumination-induced RR features observed with $\lambda_{ex} = 820$ nm are due exclusively to Chl_Z^+ and that the presence of Car^+ has no effect on the RR features of Chl_Z^+.

Figure 6 shows the SERDS data obtained for Mn-depleted PSII at 30 K after illumination at 30, 77, or 120 K. Again, the top trace depicts the control and is the same data as those shown in Figures 4 (bottom trace) and 5 (top trace). Inspection of the RR data obtained after 77 K illumination reveals that the illumination-induced signals are significantly attenuated compared with those resulting from illumination at 30 K. For example, the intensity of the SERDS feature at ~1480 cm^{-1} observed with 77 K illumination (Figure 6, middle trace) is approximately half that observed with 30 K illumination (Figure 6, top trace). With 120 K illumination (Figure 6, bottom trace), the ~1480 cm^{-1} feature is barely discernible. These results are generally consistent with a diminished yield of Chl_Z^+ at higher temperatures as indicated by the optical studies (vide supra).

It is of interest to determine whether the type of radical generated by steady-state illumination is fixed by the frozen protein conformation in a given PSII center, or whether the radical yields reflect the relative electron-transfer rates of competing electron donors. A second illumination of the protein after a portion of the cation radicals has decayed can differentiate between these two mechanisms. Because Car^+ decays much more rapidly, the sample contains relatively more Chl cation radicals after a period of dark incubation. If the type of radical generated by illumination is fixed by the frozen protein conformation in a given PSII center, then reillumination should re-form mostly Car^+ to yield the same amounts of Car^+ and Chl^+ generated by the first illumination. However, if the relative electron-transfer rates of competing electron donors determine the yields, then reillumination should produce both Car^+ and Chl^+ with the same branching ratio as in the initial illumination. We found in our studies that reillumination of the sample produces mainly Car^+ to yield the same amounts of Car^+ and Chl^+ as the initial illumination (data not shown). In another experiment, it was found that reillumination of a sample after it had been warmed to 0 °C for ~24 h regenerates the same quantities of cation radicals as initially observed at a given illumination temperature. These results demonstrate that the type of radical generated by steady-state illumination is fixed by the frozen protein conformation in a given PSII center.

Previously, Hanley et al. (*31*) reported that illumination of Mn-depleted spinach PSII at 20 K results in formation of Car^+ in essentially all of the centers and that Car^+ was replaced by Chl_Z^+ upon warming the sample in darkness to 120 K. These results were not reproduced in the current study of spinach PSII membranes and *Synechocystis* PSII core complexes. In both types of samples, a mixture of Chl and Car cations was formed, irrespective of the illumination temperature or dark incubation conditions (Figures 1 and 2). We do note, however that our spinach PSII samples were not solubilized with 0.5% β-DM as in the study by Hanley et al. (*31*), but were intact PSII membranes. To investigate the origin of the differing results, a spinach PSII membrane sample was solubilized in a high-detergent (0.5% β-DM) buffer. This sample gave results similar to those reported by Hanley et al. (*31*). Illumination at 30 K yielded primarily Car^+, and subsequent warming in the dark to 120 K resulted in decay of Car^+ concomitant with Chl^+ formation (data not shown). Although we did observe some conversion of Car^+ to the 850 nm Chl cation radical in an intact spinach PSII membrane sample upon warming in the dark to 120 K (Figure 2D), the conversion occurred to a greater extent in the spinach PSII membrane sample solubilized in a high-detergent (0.5% β-DM) buffer, and both the 817 and 850 nm Chl cation radicals were formed. These results suggest that perturbations of the protein structure by high detergent concentration may affect the rates of the electron-transfer reactions leading to formation of Car^+ and Chl^+.

We also examined whether a high concentration of glycerol could affect the sample. Although it is necessary to form a good glass in order to record the near-IR absorption spectra, we found that drying a spinach PSII membrane sample onto Mylar with only 7.5% glycerol gave satisfactory results (sample prepared as in *56*). The near-IR data obtained from the sample dried onto Mylar were equivalent to those obtained for a sample in 60% glycerol (data not shown), showing that the added glycerol did not affect the sample.

DISCUSSION

In this study, the light-induced formation of Car and Chl cation radicals has been characterized in both Mn-depleted *Synechocystis* PSII core complexes and spinach PSII membranes. The two systems behave similarly in that a mixture of Car and Chl cation radicals is formed by illumination at all of the temperatures examined from 6 to 120 K. However, there are two significant differences between the plant and cyanobacterial systems. In *Synechocystis* PSII, both Car^+ and Chl^+ are formed synchronously by illumination and do not interconvert upon warming, irrespective of the illumination temperature or dark incubation conditions (Figures 2 and 5). In spinach PSII, on the other hand, there is some conversion of Car^+ to Chl^+ when the samples are warmed after illumination (Figure 2D). A more significant difference between the species is that two spectrally distinct Chl cation radicals are formed in spinach PSII, whereas only one type of Chl cation radical is formed in *Synechocystis* PSII.

These results provide insight into the alternate electron-donation pathways to $P680^+$. A model for the alternate electron-donation pathways that is consistent with our

Scheme 1: Alternate Electron-Donation Pathways in Photosystem II

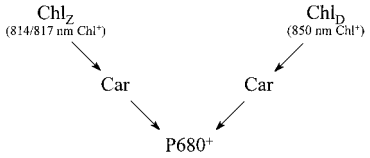

observations is shown in Scheme 1. It is based on the 2-fold symmetrical arrangement of the accessory chlorophylls called Chl_Z (ligated to D1-His118) and Chl_D (ligated to D2-His117). The locations of these accessory Chls place them each about 30 Å away from P680 (*10*), too far for rapid electron transfer without an intermediate redox-active species. There are, however, two β-carotene molecules in the D1/D2 complex (*1*) that we propose to be symmetrically arranged and to function as electron-transfer intermediates between Chl_Z/Chl_D and $P680^+$. An attractive feature of this model is that it can explain a number of seemingly contradictory observations, as will be discussed below.

The most significant difference between *Synechocystis* PSII core complexes and spinach PSII membranes is the formation of two different Chl cation radicals in the latter system. The 817 nm Chl cation radical observed in spinach PSII has an absorbance maximum close to the Chl cation radical formed in *Synechocystis* PSII and also exhibits similar formation/decay characteristics. It seems likely that the 817 and 814 nm near-IR bands observed in spinach and *Synechocystis* PSII, respectively, are from the same Chl cation radical. As discussed in the introduction, our previous studies have shown that the Chl cation radical formed in *Synechocystis* PSII is ligated to D1-H118 and, therefore, the 814/817 nm absorption band is assigned to Chl_Z^+. The 850 nm near-IR band observed in spinach PSII appears to be from a different Chl cation radical. Several lines of evidence point to the accessory Chl ligated to D2-H117 (Chl_D) as the second Chl cation radical in spinach PSII. First, the stability of the 850 nm Chl cation radical toward charge recombination argues against one of the core Chls in the D1/D2 complex. Second, the remaining Chls in PSII, other than Chl_D, are in Chl-binding proteins that are further away from the reaction center and, therefore, seem to be less likely candidates for the location of the 850 nm Chl cation radical (although a Chl in CP47 or CP43 cannot be ruled out). Third, site-directed mutations of the D2-His117 residue in *Chlamydomonas* PSII have been found to give rise to fluorescence changes that have been suggested to arise from coordination of a redox-active Chl at this position (*14*). This result contradicts the finding in *Synechocystis* PSII that D2-His117 is the axial ligand to a non-redox-active Chl residue, Chl_D (*16*). These contradictory observations can be understood if the 850 nm Chl cation radical is ligated to D2-His117. In this case, our observation that there is no formation of an 850 nm Chl cation radical in *Synechocystis* PSII would fit with the conclusion that Chl_D does not exhibit redox activity in the cyanobacterial system (*16*). On the other hand, our observation of a significant yield of the 850 nm Chl cation radical in spinach PSII fits with the conclusion that Chl_D is redox-active in the plant system (*14*).

For *Synechocystis* PSII, several observations indicate that the specific radical generated by steady-state illumination is fixed by the frozen protein conformation in a given PSII center rather than from comparable electron-transfer rates of the competing electron donors. First, the maximal yield of each radical is fixed in a given type of sample and does not change upon varying the illumination conditions or after reilluminations. For example, reillumination of a sample after allowing Car^+ to recombine in the dark at 30 K, but without warming the sample, re-forms the same amounts of Car^+ and Chl^+ as in the initial illumination; i.e., the centers in which Car^+ was formed initially only re-form Car^+. This would not be the case if there were competing pathways for electron donation with comparable rates, in which case reillumination should yield both Car^+ and Chl^+ with the same branching ratio for Car and Chl oxidation as was observed after the first illumination. Second, the rate of charge recombination of $Car^+Q_A^-$ is multiphasic (Figure 3). The presence of multiple exponential decay components shows that the samples are inhomogeneous with respect to the microscopic rate constants. This is consistent with the sample being composed of an ensemble of protein conformers that are trapped as the protein complex is frozen. Variations in the distance between Car^+ and Q_A^- could produce a range of charge-recombination rates, but it is not expected that the various conformers would have significantly different distances between the cofactors. A more likely explanation is that the ensemble of protein conformers has a distribution in the free-energy barrier for the recombination reaction that results in a distribution of rates for these electron-transfer processes. We draw analogy to the electron-transfer reactions at low temperature in the BRC in which a distribution of rates is measured owing to variations in the free energy of the reactions among the conformers in the frozen sample (*57*).

The synchronous formation of Car^+ and Chl_Z^+ in *Synechocystis* PSII during steady-state illumination could be explained in two ways. First, it is possible that Car and Chl_Z are competing donors, but that one or the other is much faster (determined by the particular conformer in the frozen sample, as discussed above). Second, it is possible that Car is the initial donor, but that there is rapid equilibration of the hole between Car and Chl_Z, resulting in localization of the hole on the lowest-potential species. The observation that $Car^+Q_A^-$ is a less stable charge-separated state than $Chl_Z^+Q_A^-$ indicates that Car may be closer to P680, and this favors the latter explanation. Accordingly, Car is positioned in Scheme 1 as the direct reductant of $P680^+$ and as an intermediate for the photooxidation of Chl_Z and Chl_D, as has also been proposed in previous models (*30, 31*). We also conclude that the synchronous formation of both Car^+ and Chl_Z^+ is due to rapid equilibration of the hole between these two donors, even at 6 K, because there is no thermally induced redistribution of the hole between Car and Chl_Z.

For spinach PSII, the formation and decay of Car^+ and Chl_Z^+ are similar to *Synechocystis* PSII. The mechanism for formation of these radicals discussed above, therefore, also applies to spinach PSII. However, spinach PSII is different with respect to having a second redox-active Chl that does not fully equilibrate with the hole on Car^+/Chl_Z^+ at temperatures of 30 K or lower because this 850 nm Chl cation radical is not completely formed unless the sample is warmed. This may be due to a longer distance and/or lower rate for electron transfer from Chl_D to Car^+. It is also possible that the reduction potential of Chl_D^+ is higher than that of

Chl_Z^+. This could occur if the keto carbonyl group of Chl_D is hydrogen bonded to a protein residue, whereas that of Chl_Z is not hydrogen bonded (*58*). Differential hydrogen-bonding interactions could also be responsible for the difference in near-IR absorption maxima of Chl_D^+ and Chl_Z^+ (*59*).

An important question is why there is a second redox-active accessory Chl in spinach PSII but only one in *Synechocystis* PSII. Based on the assignment of the 850 nm Chl cation radical to Chl_D, we examined the amino acid sequences of the D1 and D2 subunits near D1-His118 and D2-His117 for differences between spinach and *Synechocystis* (*60*). The sequence adjacent to D2-His117 is, in fact, more highly conserved than that adjacent to D1-His118. However, both Chl_Z and Chl_D are expected to be bound near small subunits associated with the D1 and D2 subunits (*10*), and it is possible that the differences between *Synechocystis* and spinach PSII result from differences in the interaction of one of these small subunits with Chl_D or the D2 subunit.

We have not included Cyt b_{559} in Scheme 1, but it is clearly involved as a secondary electron donor when PSII is illuminated at low temperatures. It has been observed for spinach PSII membranes that Cyt b_{559} is the preferential electron donor at low temperature if the heme is reduced (*24*). Although a quantitative study has not yet been carried out of the low-temperature photooxidation of Cyt b_{559} in *Synechocystis* PSII, it is known that the heme can be photooxidized at low temperature and must be preoxidized in order to observe Car and Chl photooxidation in high yield (*55*). Based on the current information, it is not possible to place Cyt b_{559} into Scheme 1 unambiguously. As described in the introduction, studies of the relative rates of photooxidation of the Mn cluster, Cyt b_{559}, and Chl_Z led to the proposal of a linear path of electron transfer from Cyt b_{559} to Chl_Z to $P680^+$ (*22*). However, recent work and the results in this paper have shown that the radical EPR signal previously attributed to Chl_Z^+ consists of three different radical species: Car^+, Chl_Z^+ and Chl_D^+. For spinach PSII membrane samples and with the illumination temperatures used in the original work (77−200 K), we can conclude that the radical EPR signal observed in (*22*) was predominantly from a Chl cation radical but was a mixture of Chl_Z^+ and Chl_D^+ (Table 1). However, if the hole equilibrates rapidly among the Car and Chl species, the specific redox center that is the immediate electron acceptor from Cyt b_{559} cannot be determined from the data in hand.

It has been argued that the observation of a thermal barrier for photooxidation of the accessory Chl requires a branching mechanism, because Cyt b_{559} can be photooxidized at low temperatures when the accessory Chl was not photooxidized (*31*). Although we have not reproduced the extent of Car^+ to Chl^+ conversion reported previously, we do observe some thermally activated hole transfer from Car^+ to Chl_D. This result would seem to rule out a linear pathway of electron transfer from $P680^+$ to Car to Chl_D to Cyt b_{559}. However, the amount of thermally activated hole transfer to Chl_D that we observe is rather small (Table 1). A careful quantitation of the yield of Car/Chl vs heme photooxidation is needed before a strong conclusion can be drawn about the intermediacy of Chl_D in the photooxidation of Cyt b_{559}. On the other hand, no Chl_D photooxidation is observed in *Synechocystis* PSII. This does not necessarily rule out a pathway for Cyt b_{559} photooxidation involving Chl_D because it is well-known that uphill electron-transfer steps can occur as long as the overall process is favorable. A good example is electron transfer within the tetraheme subunit of the reaction center from *Rps. viridis* (*61*). Time-resolved absorption measurements will be needed to ascertain the specific pathway(s) for photooxidation of Cyt b_{559} and to test the model presented in Scheme 1.

The function of the alternate electron-donation pathways in PSII is not known, but most of the recent proposals involve a role in mechanisms of protection against photoinhibition (*6*). We proposed that the reversible formation of a Chl cation radical, via the alternate electron-donation pathways, could generate a fluorescence quencher that would dissipate excitation energy under steady-state excess light (*6*, *26*). Schweitzer et al. (*19*, *20*) demonstrated that illumination of PSII at low temperature generates a radical that is a potent fluorescence quencher; similar fluorescence quenching properties were found in both cyanobacterial and spinach PSII. Based on the results in the present paper, we can conclude that Chl_Z^+ is a potent fluorescence quencher, because only Chl_Z^+ is formed in cyanobacterial PSII. Further work is needed to determine the contributions of Chl_D^+ and Car^+ to fluorescence quenching. It is interesting that the plant and cyanobacterial systems have different photoprotection mechanisms. In higher plants, the xanthophyll cycle plays an important role in photoprotection, but this cycle is absent in cyanobacteria. Our observation of differences in the alternate electron-donation processes between plant and cyanobacterial PSII may correlate with differences in the photoprotection mechanisms in these two systems and merits further study.

Finally, the different time scales for decay of the Car^+ and Chl_Z^+ near-IR absorbance bands at elevated temperatures clearly indicate the relative stability of Chl_Z^+ and instability of Car^+. When combined with the SERDS decays at elevated temperatures, these data strongly argue that the SERDS bands previously assigned to Chl_Z^+ (*16*, *42*) were correctly assigned. This observation contradicts the suggestion that the SERDS bands could arise from the influence of Car^+ on Chl_Z (*31*).

ACKNOWLEDGMENT

We thank Bruce A. Diner for providing the *Synechocystis* PCC 6803 strain.

REFERENCES

1. Gounaris, K., Chapman, D. J., Booth, P., Crystall, B., Giorgi, L., Klug, D. R., and Porter, G. (1990) *FEBS Lett. 265*, 88−92.
2. Eijckelhoff, C., and Dekker, J. P. (1995) *Biochim. Biophys. Acta 1231*, 21−28.
3. Jankowiak, R., Ratsep, M., Picorel, R., Seibert, M., and Small, G. J. (1999) *J. Phys. Chem. B 103*, 9759−9769.
4. Xiong, J., Subramaniam, S., and Govindjee. (1998) *Photosynth. Res. 56*, 229−254.
5. Debus, R. J. (1992) *Biochim. Biophys. Acta 1102*, 269−352.
6. Stewart, D. H., and Brudvig, G. W. (1998) *Biochim. Biophys. Acta 1367*, 63−87.
7. Michel, H., and Deisenhofer, J. (1988) *Biochemistry 27*, 1−7.
8. Ruffle, S. V., Donnelly, D., Blundell, T. L., and Nugent, J. H. A. (1992) *Photosynth. Res. 34*, 287−300.
9. Svensson, B., Etchebest, C., Tuffery, P., van Kan, P., Smith, J., and Styring, S. (1996) *Biochemistry 35*, 14486−14502.
10. Rhee, K.-H., Morris, E. P., Barber, J., and Kühlbrandt, W. (1998) *Nature 396*, 283−286.

11. Diner, B. A., and Babcock, G. T. (1996) in *Oxygenic Photosynthesis: The Light Reactions* (Ort, D., and Yocum, C., Eds.) pp 213−247, Kluwer Academic Publishers, Dordrecht, The Netherlands.
12. Debus, R. J. (2000) *Met. Ions Biol. Syst. 37*, 657−711.
13. Hutchison, R. S., and Sayre, R. T. (1995) in *Photosynthesis: from Light to Biosphere* (Mathis, P., Ed.) Vol. I, pp 471−474, Kluwer Academic Publishers, Dordrecht, The Netherlands.
14. Ruffle, S., Hutchison, R., and Sayre, R. T. (1998) in *Photosynthesis: Mechanisms and Effects* (Garab, G., Ed.) Vol. II, pp 1013−1016, Kluwer Academic Publishers, Dordrecht, The Netherlands.
15. Johnston, H. G., Wang, J., Ruffle, S. V., Sayre, R. T., and Gustafson, T. L. (2000) *J. Phys. Chem. B 104*, 4777−4781.
16. Stewart, D. H., Cua, A., Chisholm, D. A., Diner, B. A., Bocian, D. F., and Brudvig, G. W. (1998) *Biochemistry 37*, 10040−10046.
17. Schelvis, J. P. M., van Noort, P. I., Aartsma, T. J., and van Gorkom, H. J. (1994) *Biochim. Biophys. Acta 1184*, 242−250.
18. Koulougliotis, D., Innes, J. B., and Brudvig, G. W. (1994) *Biochemistry 33*, 11814−11822.
19. Schweitzer, R. H., and Brudvig, G. W. (1997) *Biochemistry 36*, 11351−11359.
20. Schweitzer, R. H., Melkozernov, A. N., Blankenship, R. E., and Brudvig, G. W. (1998) *J. Phys. Chem. B 102*, 8320−8326.
21. Deligiannakis, Y., Hanley, J., and Rutherford, A. W. (2000) *J. Am. Chem. Soc. 122*, 400−401.
22. Thompson, L. K., and Brudvig, G. W. (1988) *Biochemistry 27*, 6653−6658.
23. Visser, J. W. M., Rijgersberg, C. P., and Gast, P. (1977) *Biochim. Biophys. Acta 460*, 36−46.
24. de Paula, J. C., Innes, J. B., and Brudvig, G. W. (1985) *Biochemistry 24*, 8114−8120.
25. Buser, C. A., Diner, B. A., and Brudvig, G. W. (1992) *Biochemistry 31*, 11449−11459.
26. Stewart, D. H., and Brudvig, G. W. (1998) in *Photosynthesis: Mechanisms and Effects* (Garab, G., Ed.) Vol. II, pp 1113−1116, Kluwer Academic Publishers, Dordrecht, The Netherlands.
27. Schenck, C. C., Diner, B., Mathis, P., and Satoh, K. (1982) *Biochim. Biophys. Acta 680*, 216−227.
28. Yerkes, C. T., and Crofts, A. R. (1984) in *Advances in Photosynthesis Research* (Sybesma, C., Ed.) Vol. I, pp 489−492, Martinus Nijhoff/Dr W. Junk, The Hague.
29. Noguchi, T., Mitsuka, T., and Inoue, Y. (1994) *FEBS Lett. 356*, 179−182.
30. Vrettos, J. S., Stewart, D. H., de Paula, J. C., and Brudvig, G. W. (1999) *J. Phys. Chem. B 103*, 6403−6406.
31. Hanley, J., Deligiannakis, Y., Pascal, A., Faller, P., and Rutherford, A. W. (1999) *Biochemistry 38*, 8189−8195.
32. Hillmann, B., and Schlodder, E. (1995) *Biochim. Biophys. Acta 1231*, 76−88.
33. Tae, G. S., Black, M. T., Cramer, W. A., Vallon, O., and Bogorad, L. (1988) *Biochemistry 27*, 9075−9080.
34. Vallon, O., Tae, G. S., Cramer, W. A., Simpson, D., Hoyer-Hansen, G., and Bogorad, L. (1989) *Biochim. Biophys. Acta 975*, 132−141.
35. Berthold, D. A., Babcock, G. T., and Yocum, C. F. (1981) *FEBS Lett. 134*, 231−234.
36. Stewart, D. H., Nixon, P. J., Diner, B. A., and Brudvig, G. W. (2000) *Biochemistry 39*, 14583−14594.
37. Tang, X.-S., and Diner, B. A. (1994) *Biochemistry 33*, 4594−4603.
38. Palaniappan, V., Aldema, M. A., Frank, H. A., and Bocian, D. F. (1992) *Biochemistry 31*, 11050−11058.
39. Palaniappan, V., Martin, P. C., Chynwat, V., Frank, H. A., and Bocian, D. F. (1993) *J. Am. Chem. Soc. 115*, 12035−12049.
40. Shreve, A. P., Cherepy, N. J., Franzen, S., Boxer, S. G., and Mathies, R. A. (1991) *Proc. Natl. Acad. Sci. U.S.A. 88*, 11207−11211.
41. Shreve, A. P., Cherepy, N. J., and Mathies, R. A. (1992) *Appl. Spectrosc. 46*, 707−711.
42. Cua, A., Stewart, D. H., Brudvig, G. W., and Bocian, D. F. (1998) *J. Am. Chem. Soc. 120*, 4532−4533.
43. Cherepy, N. J., Shreve, A. P., Moore, L. J., Franzen, S., Boxer, S. G., and Mathies, R. A. (1994) *J. Phys. Chem. 98*, 6023−6029.
44. Cherepy, N. J., Shreve, A. P., Moore, L. J., Boxer, S. G., and Mathies, R. A. (1997) *J. Phys. Chem. B 101*, 3250−3260.
45. Cherepy, N. J., Shreve, A. P., Moore, L. J., Boxer, S. G., and Mathies, R. A. (1997) *Biochemistry 36*, 8559−8566.
46. Palaniappan, V., Schenck, C. C., and Bocian, D. F. (1995) *J. Phys. Chem. 99*, 17049−17058.
47. Czarnecki, K., Diers, J. R., Chynwat, V., Frank, H. A., and Bocian, D. F. (1997) *J. Am. Chem. Soc. 119*, 415−426.
48. Czarnecki, K., Kirmaier, C., Holten, D., and Bocian, D. F. (1999) *J. Phys. Chem. A 103*, 2235−2246.
49. Stewart, D. H., Cua, A., Bocian, D. F., and Brudvig, G. W. (1999) *J. Phys. Chem. B 103*, 3758−3764.
50. Seki, H., Arai, S., Shida, T., and Imamura, M. (1973) *J. Am. Chem. Soc. 95*, 3404−3405.
51. Tan, Q., Kuciauskas, D., Lin, S., Stone, S., Moore, A. L., Moore, T. A., and Gust, D. (1997) *J. Phys. Chem. B 101*, 5214−5223.
52. Borg, D. C., Fajer, J., Felton, R. H., and Dolphin, D. (1970) *Proc. Natl. Acad. Sci. U.S.A. 67*, 813−820.
53. Tollin, G., Castelli, F., Cheddar, G., and Rizzuto, F. (1979) *Photochem. Photobiol. 29*, 147−152.
54. Andreyeva, N. Y., Peshkin, A. F., and Chibisov, A. K. (1976) *Biofizika 21*, 29−34.
55. Stewart, D. H. (1998) Ph.D. Thesis, Yale University.
56. Lakshmi, K. V., Eaton, S. S., Eaton, G. R., and Brudvig, G. W. (1999) *Biochemistry 38*, 12758−12767.
57. Woodbury, N. W., Peloquin, J. M., Alden, R. G., Lin, X. M., Lin, S., Taguchi, A. K. W., Williams, J. C., and Allen, J. P. (1994) *Biochemistry 33*, 8089−8100.
58. Lin, X., Murchison, H. A., Nagarajan, V., Parson, W. W., Williams, J. C., and Allen, J. P. (1994) *Proc. Natl. Acad. Sci. U.S.A. 91*, 10265−10268.
59. Ivancich, A., and Mattioli, T. A. (1998) *Photosynth. Res. 55*, 207−215.
60. Svensson, B., Vass, I., and Styring, S. (1991) *Z. Naturforsch. 46C*, 765−776.
61. Chen, I.-P., Mathis, P., Koepke, J., and Michel, H. (2000) *Biochemistry 39*, 3592−3602.

BI001992O